JOURNAL OF RHEOLOGY

Using transient shear rheology to determine material parameters in fiber suspension theory

Aaron P. R. Eberle, Donald G. Baird, Peter Wapperom, and Gregorio M. Vélez-García

Citation: Journal of Rheology (1978-present) **53**, 685 (2009); doi: 10.1122/1.3099314
View online: http://dx.doi.org/10.1122/1.3099314
View Table of Contents: http://scitation.aip.org/content/sor/journal/jor2/53/3?ver=pdfcov
Published by the The Society of Rheology

Using transient shear rheology to determine material parameters in fiber suspension theory

Aaron P. R. Eberle and Donald G. Baird[a)]

Department of Chemical Engineering, Virginia Tech, Blacksburg, Virginia 24061

Peter Wapperom

Department of Mathematics, Virginia Tech, Blacksburg, Virginia 24061

Gregorio M. Vélez-García

Department of Macromolecular Science and Engineering, Virginia Tech, Blacksburg, Virginia 24061

(Received 1 September 2008; final revision received 17 February 2009)

Synopsis

Fiber suspension theory model parameters for use in the simulation of fiber orientation in complex flows are, in general, either calculated from theory or fit to experimentally determined fiber orientation generated in processing flows. Transient stress growth measurements in startup of shear flow and flow reversal in the shear rate range, $\dot{\gamma}=1-10\ s^{-1}$, were performed on a commercially available short glass fiber-filled polybutylene terephthalate using a novel "donut-shaped" sample in a cone-and-plate geometry. Predictions using the Folgar–Tucker model for fiber orientation, with a "slip" factor, combined with the Lipscomb model for stress were fit to the transient stresses at the startup of shear flow. Model parameters determined by fitting at $\dot{\gamma}=6\ s^{-1}$ allowed for reasonable predictions of the transient stresses in flow reversal experiments at all the shear rates tested. Furthermore, fiber orientation model parameters determined by fitting the transient stresses were compared to the experimentally determined evolution of fiber orientation in startup of flow. The results suggested that fitting model predictions to the stress response in well-defined flows could lead to unambiguous model parameters provided the fiber orientation as a function of time or strain at some shear rate was known. © *2009 The Society of Rheology.* [DOI: 10.1122/1.3099314]

I. INTRODUCTION

Parts made from short glass fiber composites are typically manufactured using injection or compression molding where the composite melt is forced into a mold cavity which results in the formation of a layered fiber microstructure [Advani and Sozer (2003)]. Depending on the complexity of the part and the mold filling process, local variations can arise in the fiber orientation which can severely affect the mechanical, thermal, and insulative properties of the part. As a result, it is highly desirable to be able to predict the

[a)]Author to whom correspondence should be addressed; electronic mail: dbaird@vt.edu

flow behavior of the composite fluid in connection to the fiber orientation to optimize mold design and processing conditions to maximize the part performance.

The simulation of the flow of fiber suspensions has been the subject of many publications over the past three decades. Subsequently, we give a brief introduction to the concepts relevant to this work, but for concept specifics the reader is referred to the works of Lipscomb *et al.* (1988), Bay and Tucker (1992a), and Chung and Kwon (2002b) for simulations in complex flow field geometries and Dinh and Armstrong (1984), Petrie (1999), and Sepehr *et al.* (2004a) for predictions in simple flow field geometries. We also note that fiber suspension theory has two components: an equation describing the evolution of fiber orientation and an equation for stress. For some cases, such as dilute suspensions, the two equations may be combined to form a constitutive equation. However, in most situations they are solved separately and, therefore, are discussed independently.

The theoretical framework for the evolution of fiber orientation begins with the pioneering work of Jeffery (1922). Jeffery mathematically described the motion of a single ellipsoidal particle suspended in a Newtonian fluid subjected to a Stokes flow field. This theory is easily extended to blunt-ended particles, such as fibers, using an equivalent aspect ratio of which various empirical relations have been suggested [Bretherton (1962); Cox (1971)]. For nondilute fiber suspensions Folgar and Tucker (1984) included a term to Jeffery's equation similar in formulation to isotropic diffusivity but proportional to the velocity gradient to account for fiber interaction influencing the degree of fiber alignment. Currently, there is no theoretical approach to calculate the interaction coefficient, C_I, in the Folgar–Tucker (F-T) model. For complex flow simulations, C_I has been determined by fitting simulation results to experimentally determined fiber orientation, which may not be a practical or efficient approach [Bay and Tucker (1992b)]. Empirical relations have been proposed by Bay (1991) and Phan-Thien *et al.* (2002) which indicate that C_I is a function of fiber volume fraction and aspect ratio. However, these relations have not been confirmed.

The contribution from the fiber to the bulk extra stress for dilute suspensions ($\phi < a_r^{-2}$, where ϕ is the volume fraction) arises from the hydrodynamic drag of the suspending fluid over the fiber and is well established [Hand (1961); Giesekus (1962); Batchelor (1970)]. In nondilute suspensions interparticle hydrodynamic and contact forces can significantly influence the dynamic behavior of the fiber and the stresses. The theories of Batchelor (1971), Evans (1975), Dinh and Armstrong (1984), and Shaqfeh and Fredrickson (1990) attempt to account for enhanced stress as a result of interparticle hydrodynamic interaction. The most commonly used theories in complex flow simulations are that of Dinh and Armstrong (1984) and Shaqfeh and Fredrickson (1990).

Sepehr *et al.* (2004a, 2004b) found the best agreement between simulations of the stress growth functions and experimental results for a nondilute suspension occur when the model parameters were empirically adjusted to fit the results and when a slip parameter was added to the F-T model (F-T-S). However, the feasibility of determining unambiguous material parameters by fitting was not discussed. Wang *et al.* (2008) discussed an approach to determining material parameters by fitting to the transient rheology, but the authors were unable to fit both the transient shear stress growth coefficient and the transient first normal stress difference simultaneously. As a result, the predictions were only fit to the transient shear stress growth coefficient without discussion of whether the parameters were unambiguous. Furthermore, we note that the stress growth experiments used in the comparison by Sepehr *et al.* (2004a, 2004b) and for fitting by Wang *et al.* (2008) were performed in a rotational rheometer with parallel disk geometry in which there is a varying shear rate from the center of the plates to the rim. Recent results have shown that the inhomogeneous shear field in the parallel disk geometry induces excessive

fiber-fiber interaction in concentrated fiber suspensions [Eberle *et al.* (2008a)]. This can have a severe effect on the magnitude of the stress growth overshoot peak and width of the overshoot. Also, in the model predictions presented by both Sepehr *et al.* (2004a, 2004b) and Wang *et al.* (2008) the initial fiber orientation was assumed random. However, recent results clearly show that the initial fiber orientation in rheometer samples can be closer to a planar random orientation as a result of the sample deformation history which can have a large impact on the transient predictions [Eberle (2008)].

The addition of the slip parameter to the F-T model renders the equation nonobjective. In other words, the solutions of the equation may be dependent on the external frame of reference [see, for example, Tanner (2000)]. However, the physical aspects of the predictions, in the case of simple shear flow, are still acceptable and have shown to agree with experimental rheological and simple shear injection molding data [Huynh (2001)]. Recently, Wang *et al.* (2008) proposed an objective model called the reduced-strain closure (RSC) model, which has an analogous purpose of the F-T-S model to reduce the rate of fiber reorientation. Similar to the F-T-S the RSC model is phenomenological, but focuses on the concept of reducing the growth rates of the eigenvalues without modifying the rotation rates of the eigenvectors.

For this work the F-T-S model is chosen and not the RSC because of the simple formulation and because only simple shear flow is considered. In a previous paper we showed the F-T-S can be used to accurately describe the evolution of fiber orientation in simple shear flow [Eberle (2008); Eberle *et al.* (2008b)]. However, we do note that the same concepts of determining material parameters via fitting transient rheological data could apply to the RSC model. The objective of this paper is to define an approach for determining unambiguous model parameters for the F-T-S model combined with the Lipscomb stress equation by fitting model predictions to transient shear rheological experiments performed using a donut sample in a cone-and-plate (CP) rheometer. In particular, stress growth measurements in the startup of simple shear flow and flow reversal were performed on a 30 wt % short glass fiber-filled polybutylene terephthalate (PBT-30) at various shear rates. The transient rheology is discussed with the intention of determining at which shear rate the rheological material functions should be measured and then fit. The Lipscomb model combined with the F-T-S model for fiber orientation, with experimentally determined initial conditions for fiber orientation, is fit to the stress growth behavior at a shear rate of 6 s^{-1}. The same model parameters are later used to predict the stress growth behavior at other shear rates. The equation for fiber orientation using the fit model parameters is directly compared to measurements of fiber orientation in startup of flow.

II. THEORY

A. Orientation tensors

The use of orientation tensors has become the conventional method for describing the average orientation state of a distribution of fibers. The second- and fourth-order orientation tensors, $\mathbf{A}$ and $\mathbf{A}_4$, respectively, have been defined as the second and fourth moments of the orientation distribution function, $\psi(\mathbf{u},t)$ [Advani and Tucker (1987)]

$$\mathbf{A}(t) = \int \mathbf{uu}\psi(\mathbf{u},t)d\mathbf{u}, \tag{1}$$

$$\mathbf{A}_4(t) = \int \mathbf{uuuu}\psi(\mathbf{u},t)d\mathbf{u}, \tag{2}$$

where $\mathbf{u}$ is a unit vector parallel to the backbone of each fiber. $\mathbf{A}$ is symmetric and has a trace equal to 1. For a completely random orientation state $\mathbf{A}=1/3\ \mathbf{I}$, where $\mathbf{I}$ is the unity tensor and in the limit that all the fibers are perfectly aligned in the x_1 direction the only nonzero component of $\mathbf{A}$ is $A_{11}=1$.

B. Orientation evolution equation

The common approach to predicting the motion of a single fiber begins with Jeffery's equation derived for non-Brownian axisymmetric particles [Jeffery (1922)]. For a large population of similar noninteracting particles whose orientation is represented with the orientation tensors, the time evolution of $\mathbf{A}$ can be written as [Advani and Tucker (1987)]

$$\frac{D\mathbf{A}}{Dt} = (\mathbf{W}\cdot\mathbf{A} - \mathbf{A}\cdot\mathbf{W}) + B(\mathbf{D}\cdot\mathbf{A} + \mathbf{A}\cdot\mathbf{D} - 2\mathbf{D}{:}\mathbf{A}_4), \tag{3}$$

where $D\mathbf{A}/Dt$ is the material derivative, B is a constant that depends on the aspect ratio, a_r, of the particle $B=(a_r^2-1)/(a_r^2+1)$, $\mathbf{W}=[(\boldsymbol{\nabla v})^t-\boldsymbol{\nabla v}]/2$ is the vorticity, $\mathbf{D}=[\boldsymbol{\nabla v}+(\boldsymbol{\nabla v})^t]/2$ is the rate of strain tensor, and $\boldsymbol{\nabla v}=\partial v_j/\partial x_i$. For fibers, it is common to assume the particle's aspect ratio approaches infinity, in which case $B\rightarrow 1$. The time rate of change of $\mathbf{A}$ in Eq. (3) is governed purely by the macroscopic flow field and does not include Brownian motion effects, gravity, or particle interactions, i.e., hydrodynamic or direct contact. For nondilute suspensions, Folgar and Tucker (1984) hypothesized that fiber interaction acted similarly to isotropic diffusion and as a result added a diffusionlike term to Jeffery's equation and can be written as

$$\frac{D\mathbf{A}}{Dt} = (\mathbf{W}\cdot\mathbf{A} - \mathbf{A}\cdot\mathbf{W}) + (\mathbf{D}\cdot\mathbf{A} + \mathbf{A}\cdot\mathbf{D} - 2\mathbf{D}{:}\mathbf{A}_4) + 2C_I\dot{\gamma}(\mathbf{I} - 3\mathbf{A}), \tag{4}$$

where C_I is the interaction coefficient and $\dot{\gamma}$ is the scalar magnitude of $\mathbf{D}$. The F-T model allows for the control of the steady state fiber orientation through the magnitude of C_I but the rate of fiber reorientation is still dominated by the flow field for typical values of C_I in the range of 0.016–0.0001 [Bay (1991)]. Bay (1991) developed an empirical expression for concentrated suspensions ($\phi > a_r^{-1}$),

$$C_I = 0.0184\ \exp(-0.7148\phi a_r). \tag{5}$$

Equation (5) predicts that C_I decreases for increasing ϕa_r, a result explained by a proposed caging effect. Phan-Thien *et al.* (2002) proposed a model in which C_I increases with increasing ϕa_r as

$$C_I = M[1.0 - \exp(-N\phi a_r)], \tag{6}$$

where M and N are constants. Phan-Thien *et al.* (2002) determined $M=0.03$ and $N=0.224$ by fitting Eq. (6) to experimental data by Folgar and Tucker (1984) for various suspensions of nylon fibers subject to simple shear flow. The slip parameter proposed by Sepehr *et al.* (2004a) can be incorporated into the F-T model as follows:

$$\frac{D\mathbf{A}}{Dt} = \alpha[(\mathbf{W}\cdot\mathbf{A} - \mathbf{A}\cdot\mathbf{W}) + (\mathbf{D}\cdot\mathbf{A} + \mathbf{A}\cdot\mathbf{D} - 2\mathbf{D}{:}\mathbf{A}_4) + 2C_I\dot{\gamma}(\mathbf{I} - 3\mathbf{A})], \tag{7}$$

where the slip coefficient, α, is some value between 0 and 1. As a note, the slip parameter proposed by Sepehr *et al.* (2004a) is essentially equivalent to the strain reduction factor proposed by Huynh (2001) used in complex flow simulations.

To solve Eqs. (4) and (7) a closure approximation is needed to express the fourth-order tensor $\mathbf{A}_4$ in terms of the second-order tensor. Many closure approximations have been proposed including the quadratic [Doi and Edwards (1988)], hybrid [Advani and Tucker (1987)], eigenvalue-based [Cintra and Tucker (1995)], and invariant-based optimal fitted [Chung and Kwon (2002a)]. A good review of their accuracy can be found in the works of Advani and Tucker (1990) and Chung and Kwon (2002b). For this work we use the invariant-based orthotropic fitted (IBOF) closure approximation with the fifth order polynomial coefficients for its high degree of accuracy compared to the quadratic and hybrid closures and computational efficiency compared to the eigenvalue-based closures. A complete description of the IBOF, its accuracy and polynomial coefficients, can be found elsewhere [Chung and Kwon (2002b)].

C. Stress equation

A general expression for high aspect ratio non-Brownian particles can be derived from the theories of Hand (1961) and Giesekus (1962) and is commonly referred to as the Lipscomb model [Lipscomb *et al.* (1988); Sepehr *et al.* (2004b)]

$$\boldsymbol{\sigma} = -p\mathbf{I} + 2\eta_s\mathbf{D} + 2c_1\phi\eta_s\mathbf{D} + 2\phi\eta_s N\mathbf{D}{:}\mathbf{A}_4, \tag{8}$$

where $\boldsymbol{\sigma}$ is the total stress, p is pressure, η_s is the suspending medium viscosity, c_1 is a material constant, and N is a dimensionless parameter that represents the coupling between hydrodynamic stress and fiber orientation. The third term on the right hand side of Eq. (8) is the viscosity enhancement as a result of the fibers and is similar to the enhancement term for a dilute suspension of spheres proposed by Einstein (1906). Lipscomb *et al.* (1988) gave c_1 to be equal to 2 for the limiting case of $a_r \to \infty$, but we choose to use it as a fitting parameter. The fourth term on the right hand side of Eq. (8) is the contribution to stress from the hydrodynamic drag of the fluid as it flows past a particle. Using Eq. (8) the shear stress growth coefficient, η^+, and the first normal stress growth function, N_1^+, can be written as

$$\eta^+ = \sigma_{12}/\dot{\gamma} = \eta_s + c_1\eta_s\phi + 2\eta_s\phi N A_{1212}, \tag{9}$$

$$N_1^+ = 2\phi\eta_s\dot{\gamma}N(A_{1211} - A_{1222}), \tag{10}$$

where the fourth-order tensor components are a function of time.

Subsequently, we define various theories for calculating the material coefficient N for comparison to those which were determined by fitting. For dilute suspensions ($\phi \ll a_r^{-2}$) N can be calculated from the theories of Batchelor (1971),

$$N = \frac{a_r^2}{3\ln(2a_r)}f(\varepsilon), \quad f(\varepsilon) = \frac{1 + 0.64\varepsilon}{1 - 1.5\varepsilon} + 1.659\varepsilon^2, \quad \varepsilon = [\ln(2a_r)]^{-1}, \tag{11}$$

and Lipscomb *et al.* (1988),

$$N = \frac{a_r^2}{2 \ln a_r}. \tag{12}$$

Equation (8) can also be adapted to semidilute theories ($a_r^{-2} \ll \phi \ll a_r^{-1}$) by replacing N for the dilute case to one that accounts for interparticle hydrodynamics such as the Dinh and Armstrong (1984) model

$$N = \frac{a_r^2}{3 \ln(2h/D)}, \text{ in which } h = \begin{cases} (nL^2)^{-1} & \text{random} \\ (nL)^{-1/2} & \text{aligned,} \end{cases} \tag{13}$$

where h is the interparticle spacing given for a completely random and aligned fiber orientation, D is the fiber diameter, and n is the number of fibers per unit volume. Shaqfeh and Fredrickson (1990) derived an expression for dilute and semidilute suspensions

$$N = \frac{4a_r^2}{3} \left\{ \frac{1}{\ln(1/\phi) + \ln \ln(1/\phi) + C''} \right\}, \tag{14}$$

where C'' is a constant which for randomly oriented fibers is $C''=-0.66$ and for aligned fibers $C''=0.16$. As a note, semidilute suspension theories typically neglect the third term on the right side of the equal sign in Eq. (8). As a result, when the fibers completely align themselves in the flow direction, as predicted by Jeffery's equation with $\lambda=1$, N_1^+ approaches zero and η^+ approaches the suspending medium viscosity, η.

III. EXPERIMENTAL

A. Materials

It was of a primary importance to the practical relevance of this work to use a composite fluid of industrial significance. In keeping with this material objective, a 30 wt % (volume fraction, $\phi=0.1766$) short glass fiber-filled polybutylene terephthalate (PBT-30), provided by GE Plastics under the trade name Valox 420, was used. To examine the effect of fiber concentration on the rheological behavior, PBT-30 was diluted to concentrations of 4.07, 8.42, 15, 20, and 25 wt %. Compounding was accomplished by passing dry blended amounts of PBT-30 and the neat matrix through the extruder section of an Arburg Alrounder 221-55-250 injection molder at an 200 rpm. To maintain a uniform shear and thermal history between concentrations the PBT-30 was also passed through the extruder before testing. The extrudate was collected before entering the runner of the mold and pelletized. The pellets were then compression molded for rheological testing to a CP geometry sample at 260 °C. Precautions were taken to minimize the degree of thermo-oxidative degradation of the polybutylene terephthalate (PBT) matrix by drying the materials at 120 °C for a minimum of 12 h in a vacuum oven at a pressure smaller than 0.4 in Hg before sample extrusion, molding, or testing.

To characterize the glass fiber within the suspension, pyrolysis was performed on the PBT-30 pellets at 500 °C after extrusion to separate the fibers from the matrix. The fiber length was determined by randomly measuring the length of 1000 fibers. The number average and weight average fiber length of PBT-30 was found to be $L_n=0.3640$ and $L_w=0.4388$ mm, respectively. The same fiber length measurement was performed on all the diluted concentrations and was found to be slightly higher for these concentrations and within $0.3640 \leq L_n \leq 0.3740$ and $0.4388 \leq L_w \leq 0.4578$ mm. In general, the average fiber length increased slightly for decreasing fiber concentration and is attributed to attrition from abrasive contact between fibers, which is more prevalent at higher concentrations. The fiber diameter was determined directly from images taken of fiber cross sections

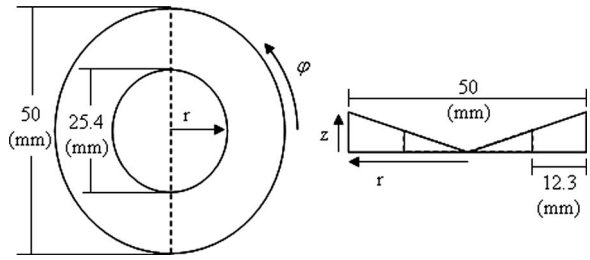

FIG. 1. Schematic drawing and cross-sectional profile of the donut sample.

using a confocal laser microscope, discussed later, and the average diameter of 1000 fibers was found to be $D=12.9\ \mu$m. This relates to a number average aspect ratio for PBT-30 of $a_r \cong 28.2$.

B. Rheological measurements

All rheological measurements were performed on a Rheometrics Mechanical Spectrometer (RMS-800) at 260 °C. To minimize the degree of thermo-oxidative degradation, all experiments were performed in a nitrogen environment with a freshly loaded preformed sample. Rheological measurements on the PBT matrix and the glass fiber-filled PBT were performed with 25 and 50 mm CP fixtures, respectively, both of which had a 0.1 rad cone angle. For the fiber-filled PBT, donut-shaped samples were used to eliminate the interaction of the fibers with the plate walls near the center of the plates where the rheometer gap is small compared to the fiber length. The dimensions of the donut sample can be seen in Fig. 1 before sample loading. A detailed discussion of the donut sample design and testing can be found elsewhere [Eberle (2008); Eberle *et al.* (2008a)]. After each experiment the void space at the center was measured to account for sample loading as the gap was adjusted to proper dimensions. The hole diameter varied slightly, 23.8 ± 0.5 mm, and was accounted for when calculating the stresses for each run.

In this work we are primarily interested in the transient rheological behavior at the startup of shear flow and flow reversal following startup of flow. In the flow reversal experiments a sample was subject to startup of flow in the clockwise (CW) direction. When the stresses reached a steady state the flow was removed and reapplied in the counter clockwise direction (CCW) at the same shear rate. The quiescent period between flows in the CW and CCW directions was roughly 10 s. The experiments were limited to a maximum shear rate of $\dot{\gamma}=10\ \text{s}^{-1}$ due to transducer overload. For the measurements, η^+ and N_1^+ were calculated as functions of torque, $M(t)$, and normal force, $F(t)$, from the following equations adapted from Macosko (1994):

$$\eta^+(t) = \sigma_{12}^+/\dot{\gamma} = \frac{3M(t)}{2\pi\dot{\gamma}}(R_o^3 - R_i^3)^{-1}, \tag{15}$$

$$N_1^+(t) = \frac{2F_z(t)}{\pi}(R_o^2 - R_i^2)^{-1}, \tag{16}$$

where R_o and R_i are the outer and inner radii of the sample, respectively. The experimental reproducibility was found to be $\pm 5\%$ for η^+ and $\pm 7\%$ for N_1^+.

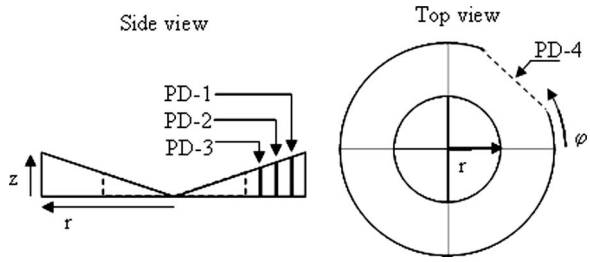

FIG. 2. Schematic drawing of the polished and imaged planes perpendicular to the neutral, r, and flow, φ, directions. Images were taken at four positions: three positions perpendicular to the flow direction at a distance of 4.0, 6.25, and 8.5 mm from the outer edge denoted by PD-1, PD-2, and PD-3, respectively, and one position perpendicular to the neutral direction denoted by PD-4.

C. Measurement of fiber orientation

The flow-induced fiber microstructure within the rheological samples was characterized using confocal laser microscopy in a similar approach to that proposed by Lee *et al.* (2002). Donut samples composed of PBT-30 were deformed using the RMS-800 at $\dot{\gamma} = 1\ s^{-1}$ for a specified amount of time. To prepare the rheometer samples for imaging, quartered sections were imbedded in epoxy to aid in sample integrity. The embedded samples were then sanded to a specific plane depth and polished to a final abrasive particle size of 0.3 μm aluminum oxide (Al_2O_3) following standardized techniques [Sawyer and Grubb (1995)]. A schematic drawing of the polished planes and locations where the images were taken can be found in Fig. 2. Each sample was imaged at two planes: perpendicular to the neutral direction x_3 and perpendicular to the flow direction x_1. A series of images was taken at three locations at distances of 4.0, 6.25, and 8.5 mm from the outer edge denoted by PD-1, PD-2, and PD-3, respectively. Images in the neutral direction were only taken at one location denoted by PD-4 at a depth of 4.0 mm from the outer edge. PD-1 and PD-4 can be considered mutually perpendicular planes of different sections of the donut sample.

Imaging was performed using a Zeiss LSM510 confocal laser scanning microscope fitted with a 40× water immersion objective lens and a laser excitation wavelength of 543 nm. The dimensions of each image were 230×230 μm with a resolution of 1024×1024 pixels. For each sample, sequential images were taken from the bottom to the top in the direction of the velocity gradient and at two planes of depth. For PBT-30 the maximum penetration was found to be 8 μm. This allowed for a three-dimensional (3D) description of the fiber orientation and removed the ambiguity associated with reflection microscopy techniques such as the Leeds method [Hine *et al.* (1993)]. In the images, the cross section of each fiber appeared as circles or ellipselike shapes. To improve the contrast between the fibers and the matrix the images were imported into power point, traced by hand, and converted to a binary image. A computer program was written and combined with image analysis software in MATLAB that measured the position of the center of mass, the major and minor axes, and local angle between the image axis and the major axis of the ellipse. The components of $\mathbf{u}$ for each fiber were determined from the elliptical "footprint" at two cross-sectional planes. A full description of this technique can be found elsewhere [Eberle (2008); Eberle *et al.* (2008b)].

In total, the fiber orientation was measured for 11 samples which corresponded to the following strains: $\gamma = 0$, 4, 7, 9, 12, 25, 50, 100, and 200. Strains 4, 25, 100, and 200 were imaged at locations PD-1 and PD-4 all other strains were imaged at locations PD-1 through PD-4 as depicted in Fig. 2. Strain 0 relates to the initial fiber orientation. In

addition, $\gamma=9$ was repeated to determine the experimental reproducibility of the analysis; the maximum error was found to be $\pm 12.4\%$ for A_{ij}. The total number of fiber cross sections counted for each sample varied depending on the strain and number of positions counted but was on the order of 1000.

With knowledge of the components of the vector $\mathbf{u}$ for each fiber, the tensors $\mathbf{A}$ and $\mathbf{A}_4$ were determined as follows:

$$A_{ij} = \frac{\sum (u_i u_j)_n F_n}{\sum F_n}, \quad F_n = \frac{M_n}{m_n}, \tag{17}$$

$$A_{ijkl} = \frac{\sum (u_i u_j u_k u_l)_n F_n}{\sum F_n}, \tag{18}$$

where M_n and m_n are the major and minor axes, respectively, of the elliptical footprint of the nth fiber cross section and F_n is a weighting factor for the nth fiber [Bay and Tucker (1992c)]. The weighting function is based on the probability of a two-dimensional plane intersecting a fiber. Meaning, a fiber aligned perpendicular to the plane is more likely to be severed than one that is aligned parallel. Using the weighting function, the larger the aspect ratio of the ellipse, the more that fiber is weighted.

IV. RESULTS AND DISCUSSION

The objective of this paper is to present an approach for determining unambiguous material parameters for fiber suspension theory by way of fitting model predictions to transient shear flow rheology coupled with knowledge of the initial fiber orientation. A dominant assumption of the theory is that the suspending medium is Newtonian, therefore, we first present the linear viscoelastic behavior of the neat PBT to confirm the Newtonian-type behavior. In addition, the first normal stress difference N_1 of the neat PBT is presented in conjunction with the PBT composite fluids containing various concentrations of short glass fiber to aid in the discussion of the contributing factors to N_1. We then present experimentally determined values of the initial fiber orientation of the rheometer samples as it is necessary to have this knowledge to accurately fit transient rheological data. This is followed by a thorough description of the transient stress growth behavior of PBT-30 following startup of flow and in flow reversal experiments at various shear rates in an attempt to determine an optimum shear rate for fitting. Finally, we present the simulation of transient shear flow at other shear rates and shear flow reversal and discuss model fitting.

A. Rheology

1. Linear viscoelastic behavior of neat PBT

The linear viscoelastic behavior of the neat suspending medium including the magnitude of the complex viscosity, $|\eta^*|$, the storage modulus, G', and loss modulus G'' vs frequency, ω, can be seen in Fig. 3. The measurement was performed at 3% strain; a strain sweep at a frequency $\omega=100$ rad/s confirmed that 3% was in the linear viscoelastic regime. The suspending medium did exhibit a storage modulus but its magnitude was small relative to the loss modulus and $|\eta^*|$ showed little dependence on frequency over the range tested (0.1–100 rad/s). Hence, the suspending medium behaved similar to a Newtonian fluid.

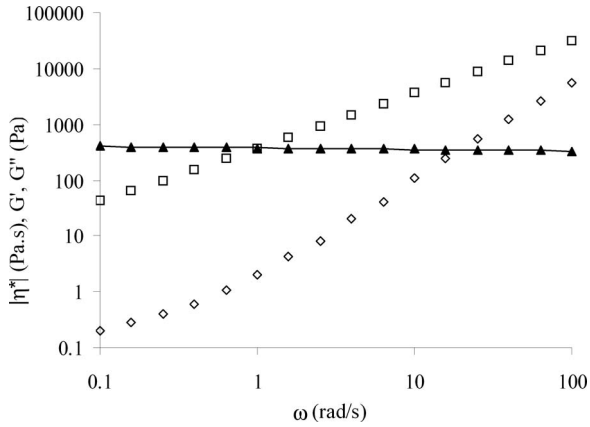

FIG. 3. The linear viscoelastic behavior of the neat PBT. The symbols (□), (◇), and (▲) represent G', G'', and $|\eta^*|$, respectively. The solid line is the Carreau–Yasuda model fit to $|\eta^*|$.

2. First normal stress difference, N_1

Many researchers have reported nonzero steady state first normal stress difference, N_1, values for fluids containing fibers which are believed not to be an enhancement to the elastic behavior of the suspending medium [Zirnsak *et al.* (1994)]. To aid in the discussion of the contributing factors to the first normal stress growth function (N_1^+), the steady state first normal stress difference, N_1, is plotted as a function of concentration in Fig. 4. The neat PBT exhibited a small N_1 of roughly 100 Pa at $\dot{\gamma}=1\ s^{-1}$. Interestingly, the addition of 4.07 wt % fiber caused a dramatic reduction in N_1 to ~2.18 Pa. This behavior coincides with the literature in that the addition of fiber seems to dramatically impede the elastic component of the suspending medium [Eberle *et al.* (2008c)]. As the concentration of fiber is increased from 4.07 to 30 wt %, N_1 appears to have a linear dependence on fiber volume fraction which is attributed to the fiber and not an enhancement of the elastic component of the suspending medium. This behavior further indicates that the suspending medium behaves in a similar manner to that of a Newtonian fluid.

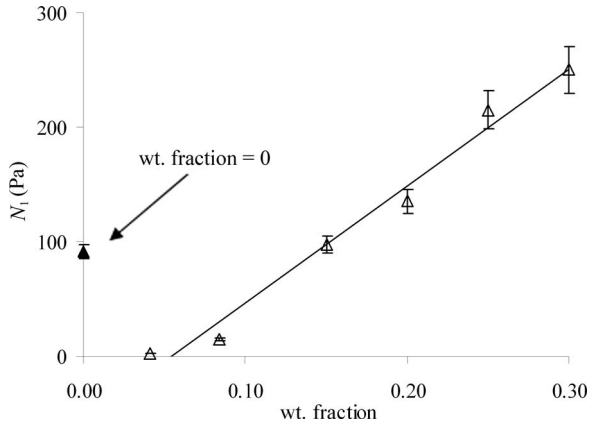

FIG. 4. N_1 as a function of fiber weight fraction at $\dot{\gamma}=1\ s^{-1}$.

3. Initial fiber orientation

The stress growth behavior of a suspension containing high aspect ratio particles is highly dependent on the initial fiber orientation distribution of the particles [Eberle *et al.* (2008a)]. This is a direct manifestation of the connection between rheology and fiber orientation. The initial fiber orientation within the donut samples represented in terms of the tensor **A** is shown in Eq. (19)

$$\boldsymbol{A}|_{\gamma=0} = \begin{pmatrix} 0.5167 & 0.0753 & 0.0584 \\ 0.0753 & 0.0349 & 0.0347 \\ 0.0584 & 0.0347 & 0.4484 \end{pmatrix}. \tag{19}$$

The experimental data represented in Eq. (19) show that the majority of the fibers were initially oriented in the flow, x_1, and neutral, x_3, directions with very few in the shear, x_2, direction. In literature it is common to assume the initial orientation is random in 3D but we find that the orientation is closer to a planar random orientation state. This is attributed to the deformation history given to the sample during compression molding of the sample disk and while the sample was loaded into the rheometer.

4. Stress growth

The rheological property of major interest is the stress growth behavior following startup of shear flow and in flow reversal experiments because of the connection between the transient stresses and the fiber orientation. In Sec. IV B we present an approach to determining model parameters by fitting the predictions to the stress growth behavior. Subsequently, we discuss the experimental stress growth behavior and its shear rate dependence to determine an optimum shear rate at which to fit the transient stresses.

The experimental values of η^+ measured during startup of flow as a function of shear rate in the range of $\dot{\gamma}=1-10\ \text{s}^{-1}$ for PBT−30 can be seen in Fig. 5(a). The magnitude of η^+ vs strain, γ, in Fig. 5(a) decreases by more than 20% over the shear rate range tested but the neat suspending medium only exhibits a 3% reduction in viscosity. The reason for the enhanced shear thinning behavior of the suspending medium is not obvious. However, one possible contributor could be local shear rate variations within close proximity of the fiber. In addition, increasing shear rates have been shown to impart a high degree of fiber orientation, effectively lowering the viscosity [Guo *et al.* (2005)]. When η^+ is normalized by the steady state viscosity, depicted in Fig. 5(b), the overshoot region of η^+/η scales in magnitude and strain for $\dot{\gamma}>1\ \text{s}^{-1}$ but for $\dot{\gamma}=1\ \text{s}^{-1}$, η^+/η exhibits a slightly enhanced behavior compared to higher shear rates. The consistent values of η^+/η at various shear rates, for $\dot{\gamma}>1\ \text{s}^{-1}$, suggest that the enhance shear thinning was a result of the suspending medium. It is not directly intuitive as to why η^+/η at $\dot{\gamma}=1\ \text{s}^{-1}$ does not scale in strain and magnitude with measurements at other shear rates.

$N_1^+/\dot{\gamma}$ vs strain is depicted in Fig. 6 for PBT-30 as a function of shear rate in the range $\dot{\gamma}=1-10\ \text{s}^{-1}$ in startup of flow. $N_1^+/\dot{\gamma}$ scales in magnitude and strain for $\dot{\gamma}>2\ \text{s}^{-1}$ but for $\dot{\gamma}\leq 2\ \text{s}^{-1}$, $N_1^+/\dot{\gamma}$ exhibits an enhanced behavior compared to higher shear rates. Similar to η^+/η it is unclear why at low shear rates, $\dot{\gamma}\leq 2\ \text{s}^{-1}$, $N_1^+/\dot{\gamma}$ exhibits an enhanced value compared to higher shear rates.

η^+ vs strain as a function of shear rate, $\dot{\gamma}=1-10\ \text{s}^{-1}$, in flow reversal following startup of flow for PBT-30 can be seen in Fig. 7(a). The shear stress growth behavior of PBT-30 at $\dot{\gamma}=6\ \text{s}^{-1}$ was added for direct comparison. Similar to the shear stress growth behavior in startup of flow, η^+ in flow reversal exhibits a transient overshoot that decays toward a steady state. However, the overshoot grows at a slower rate, resulting in an overshoot peak that occurs at a strain of ~14.7 which is more than twice the strain at which the

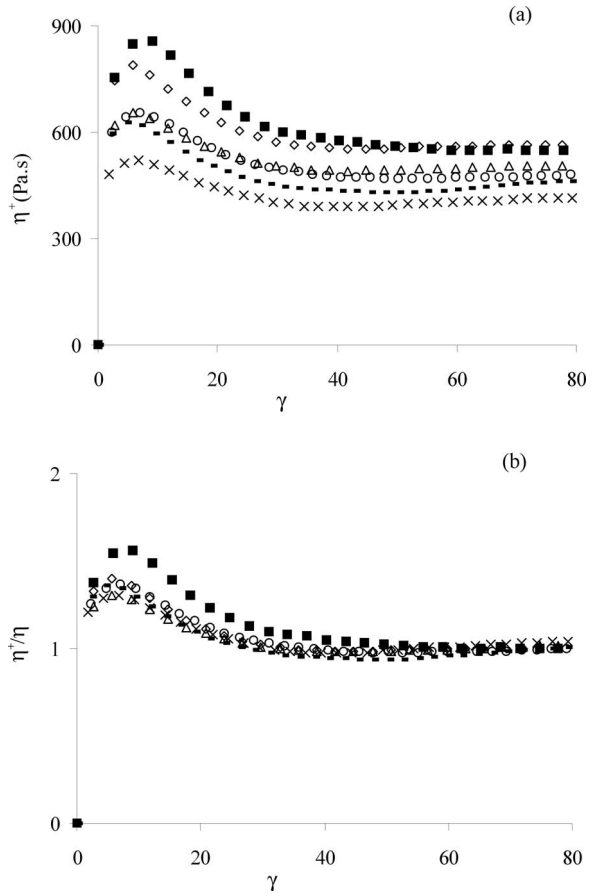

FIG. 5. Shear stress growth coefficient, η^+, as a function of shear rate $\dot{\gamma}$ for 1 (■), 2 (◇), 4 (△), 6 (○), 8 (−), and 10 s^{-1} (×). (a) η^+ and (b) η^+/η where η is the viscosity.

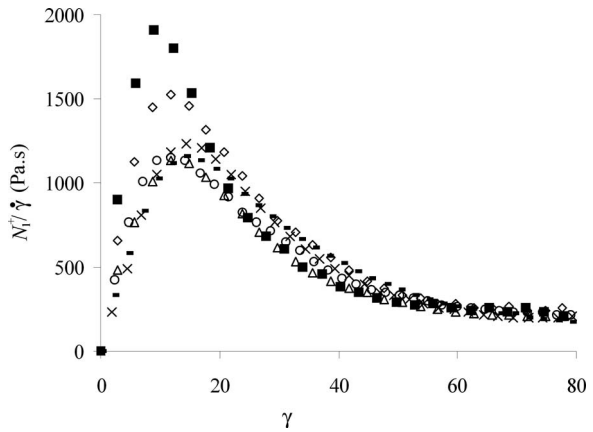

FIG. 6. First normal stress difference growth function, N_1^+, normalized by the shear rate, $\dot{\gamma}$, as a function of shear rate $\dot{\gamma}$ for 1 (■), 2 (◇), 4 (△), 6 (○), 8 (−), and 10 s^{-1} (×).

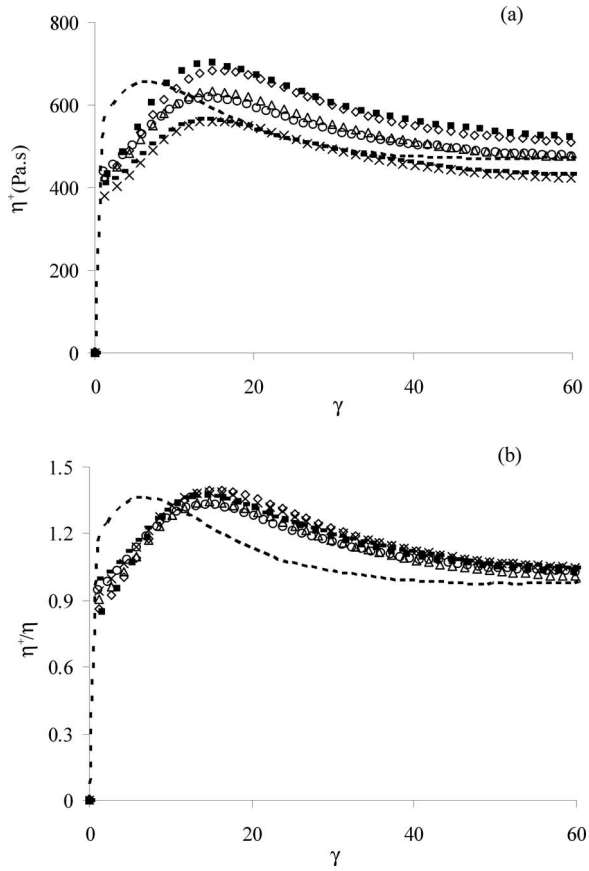

FIG. 7. Shear stress growth coefficient, η^+, in flow reversal following startup of flow as a function of shear rate $\dot{\gamma}$ for 1 (■), 2 (◇), 4 (△), 6 (○), 8 (−), and 10 s^{-1} (×). (a) η^+ and (b) η^+/η where η is the suspension viscosity. Broken line represents η^+ in startup of flow at $\dot{\gamma}=6$ s^{-1} for comparison.

peak occurred in η^+ during startup of flow. Furthermore, the magnitude of the η^+ overshoot is on average smaller for the flow reversal experiment. For example, at $\dot{\gamma}=6$ s^{-1} the reverse overshoot maximum is roughly 6% less than the initial overshoot peak, though it is within experimental error. In addition, η^+ in the flow reversal experiments decreased by more than 20% over the $\dot{\gamma}$ range tested. Figure 7(b) depicts η^+ normalized by the suspending medium viscosity, η, vs strain. Interestingly, η^+/η scales relatively well in magnitude and strain for all shear rates tested. Also, the magnitude of η^+/η in flow reversal is very similar to the magnitude of η^+/η measured in startup of flow for $\dot{\gamma} > 1$ s^{-1}.

The overshoot in η^+ measured in flow reversal experiments for suspensions containing short glass fibers has been previously reported in literature [Sepehr *et al.* (2004c)]. It is attributed to a fraction (but unspecified) of the fibers which were not completely aligned in the flow direction, rotating in the opposite direction. It is proposed that only a fraction of the fibers changes their steady state orientation because the magnitude of the overshoot is typically less than the initial overshoot. However, we find the magnitude of η^+/η in startup of flow and flow reversal to be of similar magnitude. This suggests the same mechanisms that contribute to the overshoot in startup of flow also contribute to the overshoot in flow reversal and are of similar magnitude.

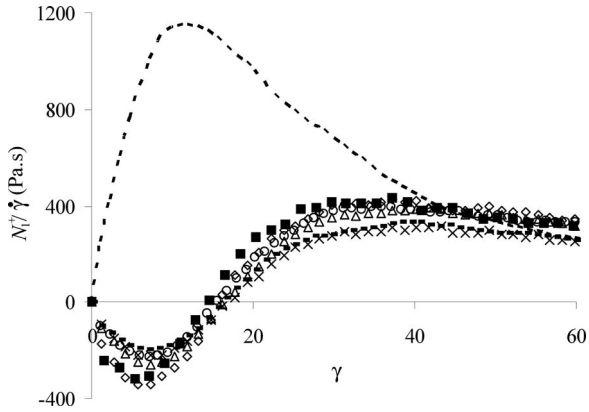

FIG. 8. First normal stress difference growth function, N_1^+, normalized by the shear rate, $\dot{\gamma}$, in flow reversal following startup of flow as a function of shear rate $\dot{\gamma}$ for 1 (■), 2 (◇), 4 (△), 6 (○), 8 (−), and 10 s^{-1} (×). Broken line represents N_1^+ in startup of flow at $\dot{\gamma}=6$ s^{-1} for comparison.

The first normal stress difference growth function normalized by the shear rate, $N_1^+/\dot{\gamma}$, as a function of $\dot{\gamma}$ in flow reversal for PBT-30 can be seen in Fig. 8. In addition, $N_1^+/\dot{\gamma}$ of PBT-30 at $\dot{\gamma}=6$ s^{-1} was added for direct comparison. $N_1^+/\dot{\gamma}$ in flow reversal behaves very differently than in startup of flow. N_1^+ initially exhibits a negative value that decreases to a minimum before increasing to a positive value where it then goes through a maximum that decays to a steady state. Similarly to η^+, the difference between $N_1^+/\dot{\gamma}$ measured at $\dot{\gamma}=1$ and 10 s^{-1} is more than 20%.

Fiber suspension theory predicts η^+x, Eq. (9), and $N_1^+/\dot{\gamma}$, Eq. (10), to be independent of shear rate for a suspension in which the suspending medium is Newtonian. A similar behavior has been shown for PBT-30 in startup of flow when η^+ is normalized by η to remove the effects of the enhanced shear thinning of the suspending medium for $\dot{\gamma}>1$ s^{-1}. The same is true for the experimental $N_1^+/\dot{\gamma}$ in which $\dot{\gamma}>2$ s^{-1}. In flow reversal $\eta^{+/}\eta$ and $N_1^+/\dot{\gamma}$ were found to be independent of shear rate for all rates tested. For fitting purposes one should choose the experimental measurements where η^+/η and $N_1^+/\dot{\gamma}$ have been confirmed to be independent of shear rate.

B. Simulation of transient shear flows

1. Numerical method and model fitting

As previously discussed and shown in Fig. 3, the neat PBT behaved similarly to a Newtonian fluid, but did exhibit a slight dependence on frequency over the range tested. For the subsequent model predictions the suspending medium viscosity, η_s, was predicted using the Carreau–Yasuda model

$$\frac{\eta-\eta_\infty}{\eta_0-\eta_\infty}=\left[1+(\lambda\dot{\gamma})^a\right]^{(n-1)/a}, \tag{20}$$

where η_0 is the zero-shear-rate viscosity, η_∞ is the infinite-shear-rate viscosity, λ is a time constant, n is the power-law exponent, a is a dimensionless parameter, and $\dot{\gamma}$ is taken equal to ω. The Carreau–Yasuda model parameters were determined by fitting to the magnitude of the complex viscosity over the frequency range of $\omega=0.1-100$ rad/s using a least-squares approach and taking $\dot{\gamma}$ to be equal to ω using the Cox–Merz rule. The

Carreau–Yasuda model fit can be seen in Fig. 3 for the following parameters: $\eta_0 = 428.2$ Pa s, $\eta_\infty = 0$ Pa s, $\lambda = 96.7$ s, $n = 0.973$, and $a = 5$.

For the equation governing the evolution of fiber orientation, Eq. (7), was solved numerically using Gears implicit predictor-corrector method at a time step of 0.01 s. The model predictions were repeated at a time step of 0.001 s for the highest $\dot{\gamma} = 10\ \text{s}^{-1}$ and the values were found to be within $\pm 10^{-4}$. Also, for Eqs. (9) and (10) the IBOF closure approximation was used to express $\mathbf{A}_4$ in terms of $\mathbf{A}$. Subsequent model predictions use Eq. (7) for the fiber orientation combined with Eqs. (9) and (10) to calculate η^+ and N_1^+, respectively. Model predictions, including the rate of fiber reorientation and magnitude of the A_{ij} components which are directly linked to the magnitude of the transient stresses, were found to be highly dependent on the initial conditions used in the model [Eberle *et al.* (2008a)]. As a result, we were only able to determine unambiguous parameters with knowledge of the fiber orientation at some point in the simulation. Model fitting without knowledge of the fiber orientation at some point led to purely ambiguous model parameters.

Simulations of η^+ using the experimentally determined initial conditions given in Eq. (19) predicts η^+ to decrease from $t = 0$. We believe that this is a deficiency in the physical predictions of Eq. (7) and is out of the scope of this paper but is discussed in detail elsewhere [Eberle *et al.* (2008b)]. As a result, the model predictions for startup of flow begin from $\gamma = 7$, the peak of the η^+ which coincides with the experimentally determined maximum in the A_{12} component. The average orientation at $\gamma = 7$ for PBT-30 was found to be

$$\boldsymbol{A}\big|_{\gamma=7} = \begin{pmatrix} 0.5457 & 0.1378 & -0.0400 \\ 0.1378 & 0.0789 & -0.0049 \\ -0.0400 & -0.0049 & 0.3754 \end{pmatrix}. \tag{21}$$

Predictions of the stress growth functions in flow reversal begin with values of orientation determined when the stresses reach steady state following the startup of shear flow.

In the model there are two fit parameters, α and C_I, for the fiber orientation in Eq. (7). α determines the rate of fiber reorientation and C_I controls the steady state fiber orientation. For the stress growth functions there are two parameters: c_1 and N. c_1 affects the magnitude of η^+ only and N controls the magnitude of η^+ and N_1^+ as a result of the hydrodynamic drag of the fluid over the fiber. Because C_I controls the steady state fiber orientation, the combination of parameters C_I, N, and c_1 must be simultaneously fit. We chose to determine these parameters by fitting the model predictions to the peak of the η^+ overshoot in addition to the steady state values of η^+ and N_1^+ measured in startup of flow. This leaves α which can be determined by simultaneously fitting the transient behavior of η^+ and N_1^+. The discussed method to fitting the model parameters was determined to be the best approach after exhausting all other possible methods. We do not include the peak of the N_1^+ overshoot in the fitting scheme because all attempts to include the peak of N_1^+ resulted in large deviations between the predicted and experimental η^+ and the onset of steady state for N_1^+. Because the parameters were determined by fitting the model to a portion of the stress growth curve, subsequently, we loosely use the term model predictions when points have been fit to specific magnitudes.

The model fit to the stress growth behavior in startup of flow and flow reversal at $\dot{\gamma} = 6\ \text{s}^{-1}$ can be seen in Figs. 9(a) and 9(b), respectively. The fit parameters can be found in Table I. In Fig. 9(a) the model predictions show reasonable agreement with the experimental results for η^+ over the complete range of strain. In contrast the model severely underpredicts the magnitude of N_1^+ in the overshoot region. The model fits of η^+ and N_1^+

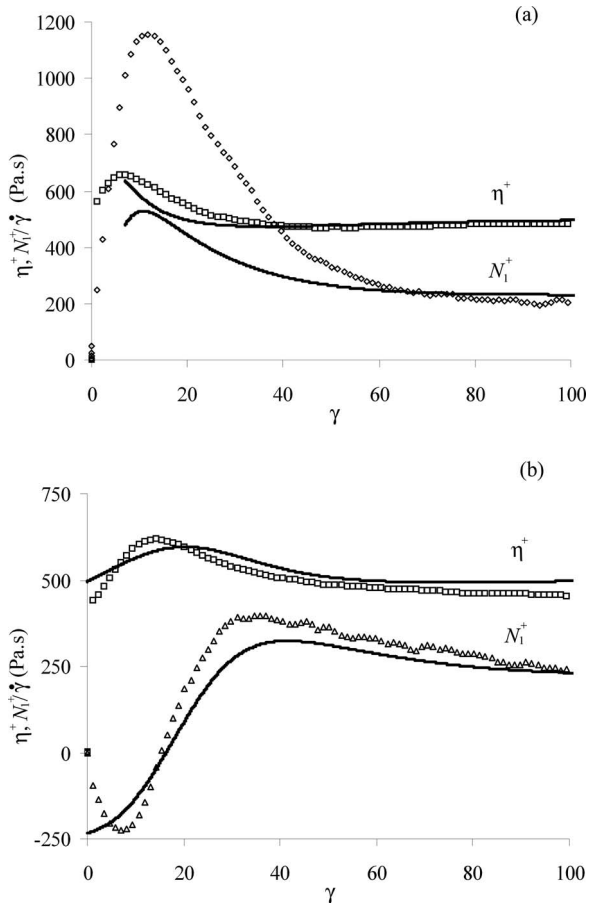

FIG. 9. Experimental results (symbols) and model predictions (solid lines) of the stress growth functions η^+ and N_1^+ in (a) startup of flow and (b) flow reversal following startup of flow at $\dot{\gamma}=6\ s^{-1}$. Model parameters can be found in Table I.

in flow reversal give good agreement with the experimental results over the complete range of strain which can be seen in Fig. 9(b). It is interesting that the model is unable to fit the large N_1^+ in startup of flow but is capable in flow reversal. This suggests that there is an additional contribution to N_1^+ in startup that is not present in flow reversal. One

TABLE I. Suspension theory fit and calculated model parameters.

	α	C_I	N	c_1
Fit to startup flow at $\dot{\gamma}=6\ s^{-1}$	0.4	0.002	27	0.4
Bay (1991)Eq. (5)		0.00052		
Phan-Thien *et al.* (2002)Eq. (6)		0.0202		
Lipscomb *et al.* (1988)Eq. (12)			119.2	
Batchelor (1971)Eq. (11)			128.1	2
Dinh and Armstrong (1984)Eq. (13)			184.4 (aligned)	
Shaqfeh and Fredrickson (1990)			653.7 (random)	
Eq. (14)			434.4 (aligned)	

plausible explanation is direct fiber contact. In startup of flow the fibers reorient from an orientation that is mostly random in the shear plan where the potential for direct fiber contact is greatest. In the flow reversal experiment, the shear history has conditioned the fibers so that they are mostly aligned in the same direction. Upon inception of flow the fibers that do rotate would most likely reorient in unison, minimizing the degree of contact. The fiber suspension theory does not include a contribution to the stresses as a result of mechanical contact.

Wang *et al.* (2008) considered a similar approach to determining material parameters by fitting solely to the transient shear stress coefficient of Valox 420. All model parameters were determined via a least-squares approach, including the contribution from the suspending medium which they found to be $\eta_s = 55.7$ Pa s. This differs considerably to the value of $\eta_s = 428.2$ Pa s used in this work. The most obvious reason as to why the values are so different is that one was determined via fitting and the other determined experimentally. The overall effect on the model predictions depends on the form of the equation for stress. In the case of Eq. (8) including η_s as a fit parameter would have rendered it impossible to determine a unique set of material parameters.

2. Model predictions

We now discuss the model predictions of the flow reversal experiments at $\dot{\gamma} = 1$ and 10 s^{-1} using the parameters determined by fitting stress growth at $\dot{\gamma} = 6$ s^{-1}. In Fig. 10(a), depicting η^+ vs γ, the model predictions show close agreement with the experimental results. At $\dot{\gamma} = 1$ s^{-1} η^+ predicts the width of the experimental overshoot and the onset of steady state but deviates slightly at the overshoot maximum. At $\dot{\gamma} = 10$ s^{-1} the predicted η^+ shows good agreement to the overshoot maximum but the onset of steady state is enhanced compared to the experimental values. The difference in the model predictions at $\dot{\gamma} = 1$ s^{-1} and $\dot{\gamma} = 10$ s^{-1} is a result of the suspending medium viscosity determined by the Carreau–Yasuda model fit to the neat suspending medium. The discrepancy between the model predictions and the experimental results for the onset of steady state of η^+ at $\dot{\gamma} = 10$ s^{-1} suggests the suspending medium viscosity is lower than the predicted value. This is a direct result of the enhanced shear thinning exhibited by the fiber suspension and not the neat suspending medium. The model predictions and experimental results for N_1^+ at $\dot{\gamma} = 1$ and 10 s^{-1} can be seen in Fig. 10(b). Predictions at both $\dot{\gamma} = 1$ and 10 s^{-1} show good agreement with the experimental results. However, in a similar fashion to η^+ the model predictions of the onset of steady state for N_1^+ at $\dot{\gamma} = 10$ s^{-1} are slightly enhanced compared to the experimental results.

We have shown that model parameters can be determined by fitting to the transient stresses in startup of flow and flow reversal. To discuss the accuracy of the fitted parameters, Fig. 11 illustrates the predictions of Eq. (7) compared to the experimentally determined fiber orientation in startup of flow at $\dot{\gamma} = 1$ s^{-1}. The predictions show reasonable agreement with the experimentally determined fiber orientation, especially at long strains which suggest that the C_I parameter is accurate. However, the model over predicts the rate of fiber reorientation which suggests the fitted α parameter is slightly too large.

To determine the accuracy of the parameters c_1 and N, associated with the magnitude of the stresses, the fourth-order tensor components in Eqs. (9) and (10) were calculated from the experimental fiber orientation. By using the experimentally determined A_{1212} with the fitted model parameters, the peak value of η^+ was found to be $\eta^+ = 876$ Pa s and the experimental $\eta^+ = 854$ Pa s. Interestingly, they are within experimental error. In contrast N_1^+ determined by using the experimentally measured $A_{1112} - A_{2212}$ with the fitted parameters was found to be $N_1^+ = 386$ Pa and the experimental $N_1^+ = 1909$ Pa. The discrep-

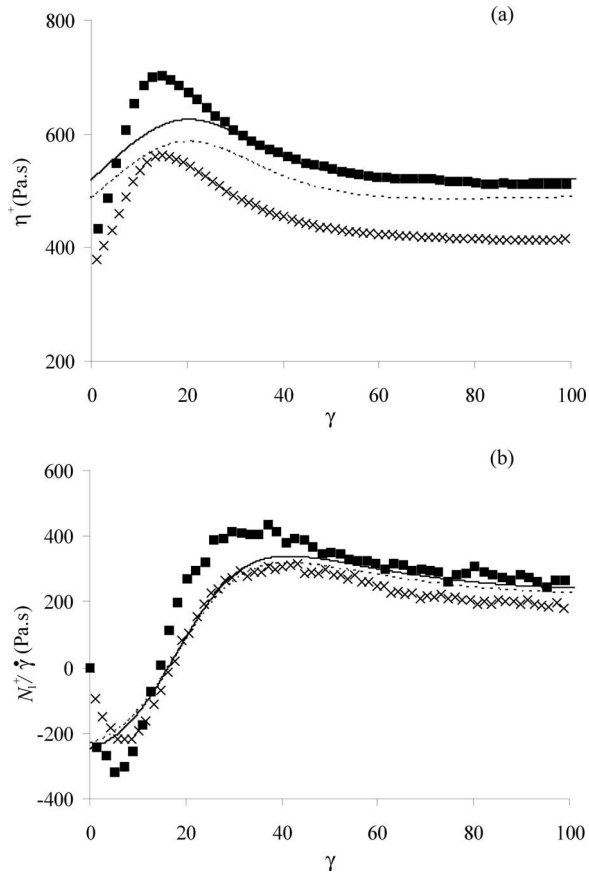

FIG. 10. Experimental predicted stress growth functions in flow reversal following startup of flow. (a) The shear stress growth coefficient, η^+, and (b) the first normal stress growth function, N_1^+. The symbols (■) and (×) represent the experimental results at $\dot{\gamma}=1$ and 10 s^{-1}, respectively, and the solid and broken lines represent the model predictions at $\dot{\gamma}=1$ and 10 s^{-1}, respectively. The fitted model parameters can be found in Table I.

ancy between the calculated N_1^+ using the fitted parameters and the measured N_1^+ is attributed to fiber contact which the model does not account for. It also suggests that η^+ can be described using simple hydrodynamic theory, while there must be additional contributing mechanisms to the overshoot in N_1^+ while the fibers are reorienting. One potential candidate could be mechanical fiber contact.

The fitted model parameters are listed in Table I along with the calculated values from theory or empirical expressions. Both the empirical expressions of Bay (1991) and Phan-Thien *et al.* (2002) give C_I values which differ by roughly 1 order of magnitude from the C_I we determined by fitting. The significance of this strongly depends on the closure approximation as it is the combination of the closure and C_I which governs the steady state fiber orientation. The constant N calculated from the various theories defined in Eqs. (12)–(14) overpredicted the magnitude N compared to the fitted value. Lipscomb's theory predicted the closest N compared to the experimental.

V. CONCLUSIONS

The objective of this work is to present an approach for determining accurate model parameters for fiber suspension theory by fitting model predictions to the transient shear

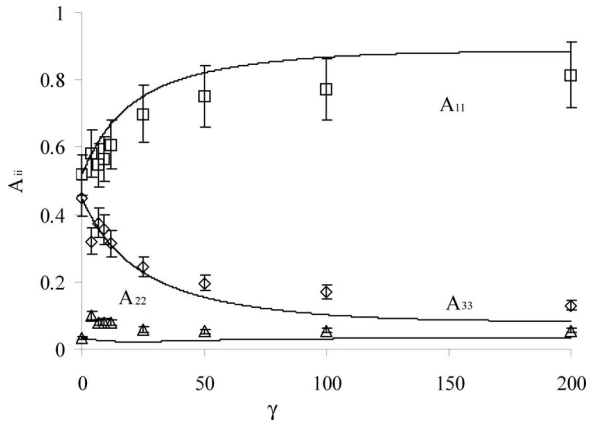

FIG. 11. Experimental and predicted fiber orientation represented through the A_{ii} components in startup of simple shear flow at $\dot{\gamma}=1\ s^{-1}$. Lines represent the model predictions of Eq. (7). Model parameters can be found in Table I.

material functions η^+ and $N_1^+/\dot{\gamma}$. To determine these parameters, first, one must determine the range of shear rates where the measured material functions η^+ and $N_1^+/\dot{\gamma}$ are independent of shear rate. Second, one must have knowledge of the fiber orientation at the startup of shear flow assuming random fiber orientation may lead to ambiguous and inaccurate parameters.

Using the parameters determined at one shear rate we were able to predict the stress growth behavior at other shear rates. However, the model for stress did not accurately predict the shear rate dependence of the viscosity. Experimentally the suspension exhibited a higher shear rate dependence than the model predicted even when the shear thinning behavior of the neat suspending medium was accounted for using the Carreau–Yasuda model. Furthermore, the model was unable to predict the magnitude of the N_1^+ overshoot in startup of flow. This was attributed to the direct fiber contact of which the model does not account for. However, we show that η^+ in startup of flow and η^+ and N_1^+ in flow reversal following startup of flow can be explained using simple hydrodynamic theory. As a result we believe this approach can lead to obtaining unambiguous and accurate model parameters. In addition we believe that fitting can lead to more accurate parameters than those determined using the available theory or empirical relations. Also, fitting allows one to determine the α parameter for which no mathematical expression currently exists. The full test of the approach will be when calculations of orientation are made in processing flows and compared against experimentally determined fiber orientation values.

ACKNOWLEDGMENTS

The financial support for this work from the National Science Foundation and Department of Energy through Grant No. DMI-0521918 is gratefully acknowledged. We thank GE Plastics for supplying the materials used in this work.

References

Advani, S. G. and E. M. Sozer, *Process Modeling in Composites Manufacturing* (Marcel Dekker, New York,

2003).
Advani, S. G. and C. L. Tucker, "The use of tensors to describe and predict fiber orientation in short fiber composites," J. Rheol. **31**, 751–784 (1987).
Advani, S. G. and C. L. Tucker, "Closure approximations for three-dimensional structure tensors," J. Rheol. **34**, 367 (1990).
Batchelor, G. K., "The stress system in a suspension of force-free particles," J. Fluid Mech. **41**, 545–570 (1970).
Batchelor, G. K., "The stress generated in a non-dilute suspension of elongated particles by pure straining motion," J. Fluid Mech. **46**, 813–829 (1971).
Bay, R. S., "Fiber orientation in injection molded composites: A comparison of theory and experiment," Ph.D. thesis, University of Illinois Urbana-Champaign, 1991.
Bay, R. S. and C. L. Tucker, "Fiber orientation in simple injection moldings. Part I: Theory and numerical methods," Polym. Compos. **13**, 317–334 (1992a).
Bay, R. S. and C. L. Tucker, "Fiber orientation in simple injection moldings. Part II. Experimental results," Polym. Compos. **13**, 332–341 (1992b).
Bay, R. S. and C. L. Tucker, "Stereological measurement and error estimates for three dimensional fibre orientation," Polym. Eng. Sci. **32**, 240–253 (1992c).
Bretherton, F. P., "The motion of rigid particles in a shear flow at low Reynolds number," J. Fluid Mech. **14**, 284–304 (1962).
Chung, D. H. and T. H. Kwon, "An invariant based optimal fitting closure approximation for the numerical prediction of flow-induced fiber orientation," J. Rheol. **46**, 169–194 (2002a).
Chung, D. H. and T. H. Kwon, "Fiber orientation in the processing of polymer composites," Korea-Aust. Rheol. J. **14**, 175–188 (2002b).
Cintra, J. S. and C. L. Tucker III, "Orthotropic closure approximations for flow-induced fiber orientation," J. Rheol. **39**, 1095–1022 (1995).
Cox, R. G., "The motion of long slender bodies in a viscous fluid. Part 2: Shear flow," J. Fluid Mech. **45**, 625–657 (1971).
Dinh, S. M. and R. C. Armstrong, "A rheological equation of state for semiconcentrated fiber suspensions," J. Rheol. **28**, 207–227 (1984).
Doi, M. and S. F. Edwards, *The Theory of Polymer Dynamics* (Oxford University Press, New York, 1988).
Eberle, A. P. R., "The dynamic behavior of a concentrated composite fluid containing non-Brownian glass fibers in rheometrical flows," Ph.D. thesis, Virginia Tech (2008).
Eberle, A. P. R., D. Baird, and P. Wapperom, "Rheology of non-Newtonian fluids containing glass fibers: A review of experimental literature," Ind. Eng. Chem. Res. **47**, 3470–3488 (2008c).
Eberle, A. P. R., D. G. Baird, P. Wapperom, and G. Velez-Garcia, "Obtaining reliable transient rheological data on concentrated short fiber suspensions using a rotational rheometer," J. Rheol., submitted (2008a).
Eberle, A. P. R., D. G. Baird, P. Wapperom, and G. M. Velez-Garcia, "Fiber orientation kinetics of a concentrated short glass fiber suspension in startup of simple shear flow," J. Non-Newtonian Fluid Mech., submitted (2008b).
Einstein, A., "A new determination of molecular dimensions," Ann. Phys. **19**, 289–306 (1906).
Evans, J. G., "The flow of a suspension of force-free rigid rods in a Newtonian fluid," Ph.D. thesis, Cambridge University, 1975.
Folgar, F. P. and C. L. Tucker, "Orientation behavior of fibers in concentrated suspensions," J. Reinf. Plast. Compos. **3**, 98–119 (1984).
Giesekus, H., "Stromungen mit konstantem Geschwindigkeitsgradienten und die Bewegung von darin suspendierten Teilchen. Teil I: Raumliche Stromungen," Rheol. Acta **2**, 101–112 (1962).
Guo, R., J. Azaiez, and C. Bellehumeur, "Rheology of fiber filled polymer melts: Role of fiber-fiber interactions and polymer-fiber coupling," Polym. Eng. Sci. **45**, 385–399 (2005).
Hand, G. L., "A theory of dilute suspensions," Arch. Ration. Mech. Anal. **7**, 81–86 (1961).
Hine, P. J., N. Davidson, R. A. Duckett, and I. M. Ward, "Measuring the fibre orientation and modeling the elastic properties of injection-moulded long-glass-fibre-reinforced nylon," Compos. Sci. Technol. **53**, 125–131 (1995).

Huynh, H. M., "Improved fiber orientation predictions for injection-molded composites," MS thesis, University of Illinois at Urbana-Champaign (2001).

Jeffery, G. B., "The motion of ellipsoidal particles immersed in a viscous fluid," Proc. R. Soc. London, Ser. A **102**, 161–179 (1922).

Lee, Y., S. Lee, J. Youn, K. Chung, and T. Kang, "Characterization of fiber orientation in short fiber reinforced composites with an image processing technique," Mater. Res. Innovations **6**, 65 (2002).

Lipscomb, G. G., M. M. Denn, D. U. Hur, and D. V. Boger, "The flow of fiber suspensions in complex geometries," J. Non-Newtonian Fluid Mech. **26**, 297–325 (1988).

Macosko, C. W., *Rheology Principles, Measurements, and Applications* (Wiley, New York, 1994).

Petrie, C. J. S., "The rheology of fibre suspensions," J. Non-Newtonian Fluid Mech. **87**, 369–402 (1999).

Phan-Thien, N., X.-J. Fan, R. I. Tanner, and R. Zheng, "Folgar–Tucker constant for fiber suspension in a Newtonian fluid," J. Non-Newtonian Fluid Mech. **103**, 251–260 (2002).

Sawyer, L. C. and D. Grubb, *Polymer Microscopy* (Springer, New York, 1995).

Sepehr, M., G. Ausias, and P. J. Carreau, "Rheological properties of short fiber filled polypropylene in transient shear flow," J. Non-Newtonian Fluid Mech. **123**, 19–32 (2004a).

Sepehr, M., P. J. Carreau, M. Grmela, G. Ausias, and P. G. Lafleur, "Comparison of rheological properties of fiber suspensions with model predictions," J. Polym. Eng. **24**, 579–610 (2004b).

Sepehr, M., P. J. Carreau, M. Moan, and G. Ausias, "Rheological properties of short fiber model suspensions," J. Rheol. **48**, 1023–1048 (2004c).

Shaqfeh, E. S. G. and G. H. Fredrickson, "The hydrodynamic stress in a suspension of rods," Phys. Fluids A **2**, 7–25 (1990).

Tanner, R. I., *Engineering Rheology* (Oxford University Press, New York, 2000).

Wang, J., J. F. O'Gara, and C. L. Tucker, "An objective model for slow orientation kinetics in concentrated fiber suspensions: Theory and rheological evidence," J. Rheol. **52**, 1179–1200 (2008).

Zirnsak, M. A., D. U. Hur, and D. V. Boger, "Normal stresses in fibre suspensions," J. Non-Newtonian Fluid Mech. **54**, 153–193 (1994).